

Underdoped cuprates phenomenology in the 2D Hubbard model within COM(SCBA)

Adolfo Avella* and Ferdinando Mancini†

*Dipartimento di Fisica “E.R. Caianiello” - Unità CNISM di Salerno
Università degli Studi di Salerno, I-84081 Baronissi (SA), Italy*

(Dated: July 25, 2006)

The two-dimensional Hubbard model is studied within the Composite Operator Method (COM) with the residual self-energy computed in the Self-Consistent Born Approximation (SCBA). COM describes interacting electrons in terms of the new elementary excitations appearing in the system owing to strong correlations; residual interactions among these excitations are treated within the SCBA. The anomalous features appearing in the spectral function $A(\mathbf{k}, \omega)$, the momentum distribution function $n(\mathbf{k})$ and the Fermi surface are analyzed for various values of the filling (from overdoped to underdoped region) in the intermediate coupling regime at low temperatures. For low doping, in contrast with the ordinary Fermi-liquid behavior of a weakly-correlated metal found at high doping, we report the opening of a pseudogap and some non-Fermi-liquid features as measured for cuprates superconductors. In addition, we show the presence of kinks in the calculated electronic dispersion in agreement with ARPES data.

PACS numbers: 71.10.Fd, 71.27.+a, 71.10.-w

One of the most intriguing challenges in modern condensed matter theory is the description of the anomalous behaviors experimentally observed in novel materials. By anomalous behaviors we mean those not predicted by standard many-body theory, that is, behaviors in contradiction with Fermi-liquid framework and diagrammatic expansions. Underdoped cuprates superconductors display anomalous features in almost all experimentally measurable physical properties [1, 2, 3]. As a matter of fact, the microscopic description of this class of materials is still an open problem because many of the anomalous features remain unexplained or, at least, controversially debated [4, 5]: non-Fermi-liquid response, quantum criticality, pseudogap formation, ill-defined Fermi surface, and kinks in electronic dispersion.

Since the very beginning [6], the two-dimensional Hubbard model [7] has been recognized as the minimal model capable to describe the $Cu - O_2$ planes of cuprates superconductors. It certainly contains many of the key ingredients by construction: strong electronic correlations, competition between localization and itineracy, Mott physics, and low-energy spin excitations. Unfortunately, although fundamental for benchmarking and fine tuning analytical theories, numerical approaches [8] can be of little help to solve the puzzle of cuprates owing to their limited resolution in frequency and momentum. On the other hand, there are not so many analytical approaches capable to deal with the quite complex aspects of underdoped cuprates phenomenology. Among others, the most promising approaches available in the literature are the cellular dynamical mean-field theory [9], the dynamical cluster approximation [10], and the cluster perturbation theory [11]. Anyway, it is worth noticing that all these approaches cannot avoid relying on some numerical method in order to close their self-consistency cycles.

In this manuscript, we show that the two-dimensional Hubbard model within a completely analytical self-

consistent approach, the Composite Operator Method (COM) [12] with the residual self-energy computed in the Self-Consistent Born Approximation (SCBA) [13], can describe many of the anomalous features contributing to the experimentally observed underdoped cuprates phenomenology. In particular, we show how Fermi arcs develop out of a large Fermi surface, how pseudogap shows itself in the dispersion and in the density of states, how non-Fermi liquid features become apparent in the momentum distribution function, and how much *kinked* can get the dispersion on varying doping. The manuscript is organized as follows: first, we recall the Hubbard model and fix the notation; then, we present the Composite Operator Method and its application to the system under analysis; finally, we present results and comparisons with experiments and give conclusions.

The two-dimensional Hubbard model reads as

$$H = \sum_{\mathbf{ij}} (-\mu \delta_{\mathbf{ij}} - 4t \alpha_{\mathbf{ij}}) c^\dagger(i) c(j) + U \sum_{\mathbf{i}} n_\uparrow(i) n_\downarrow(i) \quad (1)$$

where $c^\dagger(i) = (c^\dagger_\uparrow(i), c^\dagger_\downarrow(i))$ is the creation electronic operator in spinorial notation and Heisenberg picture ($i = (\mathbf{i}, t_i)$), \mathbf{i} is a vector of the Bravais lattice, $n_\sigma(i) = c^\dagger_\sigma(i) c_\sigma(i)$ is the spin- σ electronic number operator, μ is the chemical potential, t is the hopping integral and the energy unit, U is the Coulomb on-site repulsion, $c^\alpha(\mathbf{i}) = \sum_{\mathbf{j}} \alpha_{\mathbf{ij}} c(\mathbf{j})$ and $\alpha_{\mathbf{ij}}$ is the projector on the nearest-neighbor sites.

COM recipe uses three main ingredients [12]: *composite* operators, *algebra* constraints, and *residual* interactions treatment. Composite operators are products of electronic operators and describe the new elementary excitations appearing in the system owing to strong correlations. According to the system under analysis [12], you have to choose a set of composite operators as operatorial basis and rewrite the electronic operators and

the electronic Green's function in terms of this basis. You should think of composite operators just as a better point, with respect to electronic operators, where to start your mean field approximation. Algebra constraints are relations among correlation functions dictated by the non-canonical operatorial algebra closed by the chosen operatorial basis [12]. After choosing an operatorial basis, one way to obtain algebra constraints is to check which correlation functions of two elements of the basis (named correlators hereafter) vanish or can be expressed in terms of other correlators according to the operatorial algebra closed by the basis. Other ways to obtain algebra constraints rely on the symmetries enjoined by the Hamiltonian under study, the Ward-Takahashi identities, the hydrodynamics, etc [12]. You should think of algebra constraints as a way to restrict the Fock space on which the chosen operatorial basis acts to the Fock space of physical electrons. Algebra constraints are used to compute unknown correlation functions appearing in the calculations. Residual interactions among the elements of the chosen operatorial basis are described by the residual self-energy, that is, the propagator of the residual term of the current after this latter has been projected on the chosen operatorial basis [12]. According to the physical properties under analysis and the range of temperatures, dopings, and interactions you wish to explore, you have to choose an approximation to compute the residual self-energy. You should think of residual self-energy as a measure in the frequency and momentum space of how much well defined, as quasi-particles, are your composite operators.

Following COM prescriptions [12], we have chosen as operatorial basis $\psi^\dagger(i) = (\xi^\dagger(i), \eta^\dagger(i))$, with $\eta(i) = n(i)c(i)$ and $\xi(i) = c(i) - \eta(i)$, guided by the hierarchy of the equations of motion and by the exact solution of the Hubbard Hamiltonian reduced to its interacting term. The retarded Green's function $G(i, j) = \langle R[\psi(i)\psi^\dagger(j)] \rangle$ has the following expression in terms of the two-pole propagator $G^0(\mathbf{k}, \omega)$

$$G(\mathbf{k}, \omega) = (IG^0(\mathbf{k}, \omega)^{-1} - \Sigma(\mathbf{k}, \omega)I^{-1})^{-1}I \quad (2)$$

where $\Sigma = \mathcal{F}\langle R[\delta J(i)\delta J^\dagger(j)] \rangle_I$ stands for the irreducible part of the residual self-energy and \mathcal{F} for the Fourier transform. Till further notice, all objects appearing in the equations stands for two by two matrices, according to the vectorial nature of the operatorial basis. The entries of the normalization matrix $I = \langle \{\psi(\mathbf{i}, t), \psi^\dagger(\mathbf{j}, t)\} \rangle$ read as: $I_{11} = 1 - I_{22}$, $I_{22} = n/2$ and $I_{12} = I_{21} = 0$. n is the filling. The two-pole propagator $G^0(\mathbf{k}, \omega)$ has the following expression

$$G^0(\mathbf{k}, \omega) = (\omega - \varepsilon(\mathbf{k}))^{-1}I \quad (3)$$

where $\varepsilon(\mathbf{k})$ is the energy matrix appearing in the projected equations of motion of $\psi(i)$

$$i\frac{\partial}{\partial t}\psi(\mathbf{k}, t) = [\psi(\mathbf{k}, t), H] = \varepsilon(\mathbf{k})\psi(\mathbf{k}, t) + \delta J(\mathbf{k}, t) \quad (4)$$

once the constraint $\langle \{\delta J(\mathbf{i}, t), \psi^\dagger(\mathbf{j}, t)\} \rangle = 0$ has been enforced. This constraint assures that the residual current $\delta J(i)$ describe the physics *orthogonal* to the chosen operatorial basis $\psi(i)$; that is, $\delta J(i)$ describes the interactions among the elements of the operatorial basis.

Three parameters appear in the energy matrix $\varepsilon(\mathbf{k})$: the chemical potential μ , the difference between upper and lower intra-subband contributions to kinetic energy $\Delta = \langle \xi^\alpha(i)\xi^\dagger(i) \rangle - \langle \eta^\alpha(i)\eta^\dagger(i) \rangle$, and a combination of the nearest-neighbor charge-charge, spin-spin and pair-pair correlation functions $p = \frac{1}{4}\langle \delta n_\mu^\alpha(i)\delta n_\mu(i) \rangle - \langle [c_\uparrow(i)c_\downarrow(i)]^\alpha c_\downarrow^\dagger(i)c_\uparrow^\dagger(i) \rangle$. $\delta n_\mu(i) = n_\mu(i) - \langle n_\mu(i) \rangle$ stands for charge ($\mu = 0$) and spin ($\mu = 1, 2, 3$) number operators and the sum over repeated indices is understood. By exploiting algebra constraints and connections between propagators and correlators, we have fixed the parameters appearing in the energy matrix through a set of three self-consistent equations. Two equations are obtained by expressing the filling n and the parameter Δ in terms of correlators, respectively. The third equation is the algebra constraint $\langle \xi(i)\eta^\dagger(i) \rangle = 0$ that excludes double occupancy of a site by two electrons with the same spin.

We have chosen to compute the residual self-energy $\Sigma(\mathbf{k}, \omega)$ within SCBA [12, 14, 15]. According to this, we have

$$\Sigma(\mathbf{k}, \omega) = 4t^2 I^{-1} S(\mathbf{k}, \omega) (1 - \sigma_x) I^{-1} \quad (5)$$

with $S(\mathbf{k}, \omega) = \mathcal{F}_\mathbf{k}[S(\mathbf{r}, \omega)]$ and

$$S(\mathbf{r}, \omega) = \iint \frac{d\omega' d\Omega}{(2\pi)^2} \frac{1 + e^{-\beta\omega'}}{\omega - \omega' + i\varepsilon} F(\mathbf{r}, \Omega) B(\mathbf{r}, \omega' - \Omega) \quad (6)$$

where

$$F(\mathbf{i} - \mathbf{j}, \omega) = \mathcal{F}_\omega \langle c^\alpha(i)c^{\dagger\alpha}(j) \rangle \quad (7)$$

and

$$B(\mathbf{i} - \mathbf{j}, \omega) = \mathcal{F}_\omega \langle \delta n_\mu(i)\delta n_\mu(j) \rangle \quad (8)$$

and \mathcal{F}_ω and $\mathcal{F}_\mathbf{k}$ are the time-frequency and position-momentum Fourier transform operators, respectively. σ_x is the first Pauli matrix.

We have decided to compute both charge-charge and spin-spin propagators (8) within the two-pole approximation [12, 16] instead of using model spin susceptibilities [17]. We have chosen charge and spin number operators $n_\mu(i)$ and their currents $\rho_\mu(i) = c^\dagger(i)\sigma_\mu c^\alpha(i) - c^{\dagger\alpha}(i)\sigma_\mu c(i)$ as operatorial basis. $\sigma_\mu = (1, \sigma)$ and σ are the Pauli matrices. Within this framework, the bosonic propagators depend on both electronic correlators and high-order bosonic correlation functions, one per each channel, named a_c and a_s [12, 16]. We have fixed a_c and a_s through the algebra constraints $\langle n(i)n(i) \rangle = n + 2D$

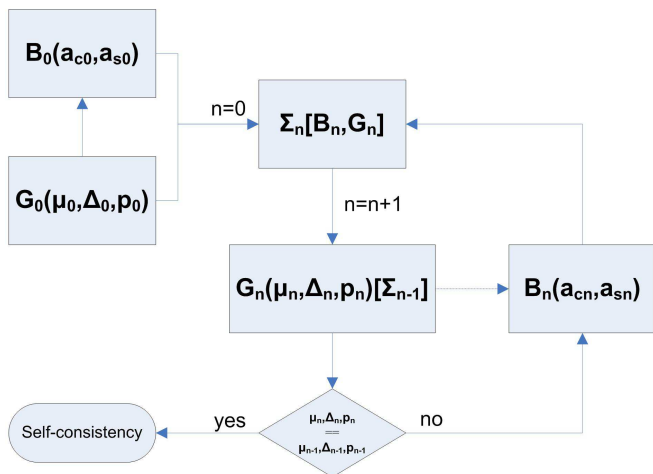


FIG. 1: Self-consistency scheme to compute the propagator G in terms of the charge-charge and spin-spin propagator B and the residual self-energy Σ .

and $\langle n_z(i)n_z(i) \rangle = n - 2D$, where D is the double occupancy, that excludes double occupancy of a site by two electrons with the same spin and enforces the relation between filling and *length* of the electronic spin on the same site, respectively.

The propagator G is computed through the self-consistency scheme depicted in Fig. 1: we first compute G_0 and B_0 in two-pole approximation, then Σ and consequently G . Finally, we check how much the fermionic parameters (μ , Δ and p) changed and decide if to stop or to continue by computing new B and Σ after G and so on. To get 6-digit precision for fermionic parameters, we usually need about 10 cycles (it varies very much with doping, temperature and interaction strength) on a 3D grid of 128×128 points in momentum space and 4096 Matsubara frequencies.

In Fig. 2, we report the electronic spectral function at the chemical potential $A(\mathbf{k}, \omega = 0) = -\frac{1}{\pi} \Im [G_{cc}(\mathbf{k}, \omega = 0)]$ as a function of momentum \mathbf{k} for $U = 8$, $n = 0.78$ and $T = 0.01$ (right panel), $n = 0.85$ and $T = 0.01$ (middle panel) and $n = 0.92$ and $T = 0.02$ (left panel). $G_{cc} = G_{11} + G_{12} + G_{21} + G_{22}$ is the electronic Green's function. The maxima of $A(\mathbf{k}, \omega = 0)$ mark the effective Fermi surface as measured by ARPES. The solid line marks the level 0.5 of the electronic momentum distribution function $n(\mathbf{k})$ per spin, that is, the Fermi surface in a perfect Fermi liquid. The dashed line marks the level zero of $r(\mathbf{k}) = \varepsilon_0(\mathbf{k}) + \Sigma'_{cc}(\mathbf{k}, \omega = 0)$, that is, the Fermi surface if no damping would be present. The dotted lines are labeled with the values of $\Sigma''_{cc}(\mathbf{k}, \omega = 0)$. The dashed-dotted line is a guide to the eye and marks the reduced (antiferromagnetic) Brillouin zone. $\varepsilon_0(\mathbf{k}) = -4t\alpha(\mathbf{k}) - \mu$ is the noninteracting dispersion. $\Sigma_{cc}(\mathbf{k}, \omega)$ is the electronic self-energy

$$G_{cc}(\mathbf{k}, \omega) = (\omega - \varepsilon_0(\mathbf{k}) - \Sigma_{cc}(\mathbf{k}, \omega))^{-1} \quad (9)$$

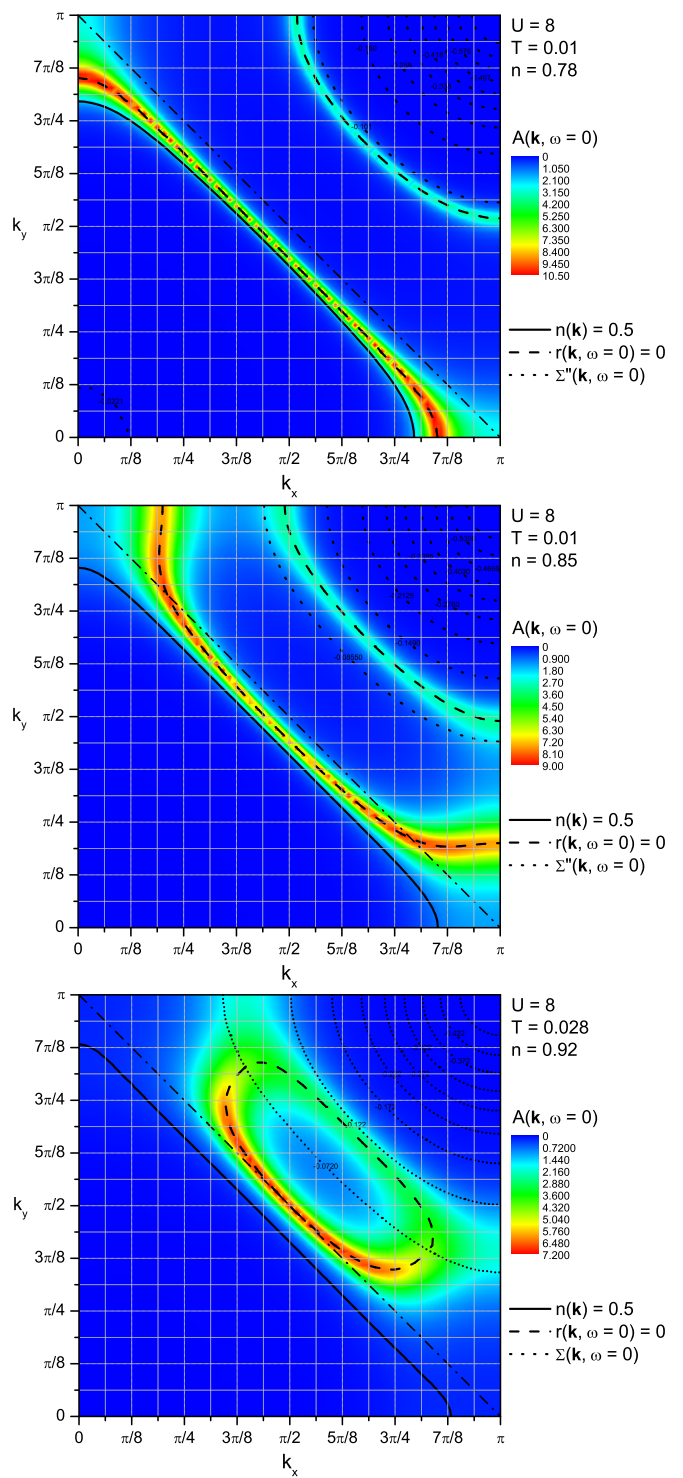


FIG. 2: Spectral function at the chemical potential $A(\mathbf{k}, \omega = 0)$ as a function of momentum \mathbf{k} for $U = 8$, (left) $n = 0.78$ and $T = 0.01$ (center) $n = 0.85$ and $T = 0.01$ (right) $n = 0.92$ and $T = 0.028$.

At large doping ($n = 0.78$), we identify a weakly-interacting Fermi metal. The Fermi surface, that marked by maxima of $A(\mathbf{k}, \omega = 0)$, is practically coincident with the level 0.5 of the momentum distribution function. The

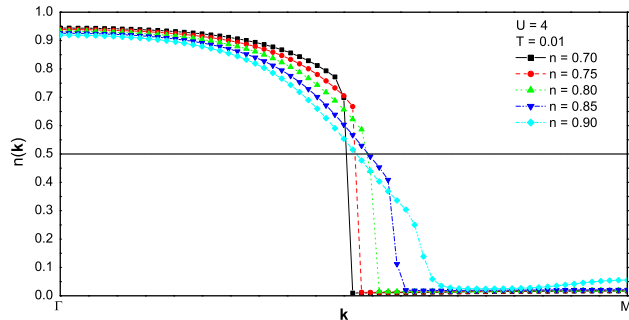


FIG. 3: Momentum distribution function $n(\mathbf{k})$ along the principal diagonal of the Brillouin zone for various fillings at $U = 4$ and $T = 0.01$.

rather low signal in proximity of $M = (\pi, \pi)$ is reminiscent of the shadow band (see Fig. 5). At $n = 0.85$, we just passed through optimal doping ($n \cong 0.82$). This latter is marked by a change in the topology of the Fermi surface between open and close and, consequently, by the coincidence between the value of the chemical potential and the position of the van Hove singularity (see Fig. 5). The chemical potential presents an inflection point at this doping (not shown) which allowed us to determine its position with accuracy. A certain discrepancy between the Fermi surface and the level 0.5 of the momentum distribution function is now clearly visible around the antinodal points ($X = (\pi, 0)$ and $Y = (0, \pi)$). At low doping ($n = 0.92$), the situation is dramatically changed and the scenario is that of a strongly-interacting antiferromagnetic metal. The Fermi surface is ill defined (it does not enclose a definite region of momentum space) and does not coincide with the level 0.5 of the momentum distribution function: we have no more a Fermi liquid. The formation of a pseudogap can be deduced by the remarkable difference between the intensities at the cold spots (the well defined arch departing from $(\pi/2, \pi/2)$, the nodal point) and the hot spots (the regions in proximity of the antinodal points). The imaginary part of the self-energy is so intense on the outer part of the hole pocket (the Fermi surface if no damping would be present) to reduce it just to an arch as reported by ARPES experiments [1]. The antiferromagnetic fluctuations are so strong to destroy the coherence of the quasi-particles in that region of momentum space.

In Fig. 3, we report the electronic momentum distribution function $n(\mathbf{k})$ per spin as a function of momentum \mathbf{k} along the principal diagonal of the Brillouin zone $\Gamma = (0, 0) \rightarrow M = (\pi, \pi)$ for various fillings at $U = 4$ and $T = 0.01$. On increasing the filling (reducing the doping) the quite sharp jump going through the level 0.5, clearly visible for $n = 0.7$, progressively moves its center downward and almost disappears for $n = 0.9$. In particular, between $n = 0.8$ and $n = 0.85$, we can clearly

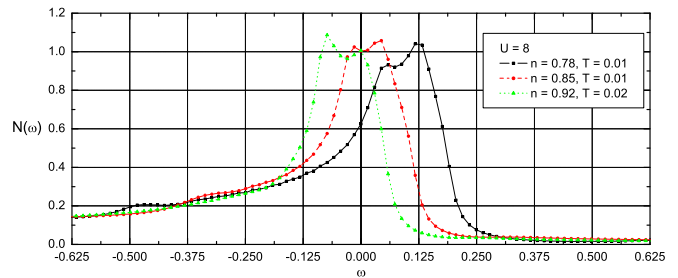


FIG. 4: Density of states for $U = 8$, (solid line) $n = 0.78$ and $T = 0.01$ (dashed line) $n = 0.85$ and $T = 0.01$ (dotted line) $n = 0.92$ and $T = 0.02$.

see the appearance of a finite slope at the level 0.5, signalling the passage from Fermi-liquid excitations to non-Fermi-liquid ones. The Fermi surface itself becomes ill defined. The formation of a hole pocket for the lowest doping is signalled by the appearance of finite weight at $M = (\pi, \pi)$.

In Fig. 4, we report the electronic density of states $N(\omega)$ per spin as a function of frequency for $U = 8$, (solid line) $n = 0.78$ and $T = 0.01$ (dashed line) $n = 0.85$ and $T = 0.01$ (dotted line) $n = 0.92$ and $T = 0.02$ in the frequency region in proximity of the chemical potential. On increasing the filling (reducing the doping) there is an evident transfer of spectral weight between the top of the dispersion band (see Fig. 5) and the antinodal points where the van Hove singularity resides. At the lowest doping ($n = 0.92$), we clearly see a well developed pseudogap below the chemical potential as a depression between two peaks, one pinned at the Fermi surface and another at the van Hove singularity.

In Fig. 5, we report the electronic spectral function $A(\mathbf{k}, \omega)$ along the principal directions ($\Gamma = (0, 0) \rightarrow M = (\pi, \pi)$, $M = (\pi, \pi) \rightarrow X = (\pi, 0)$, $X = (\pi, 0) \rightarrow Y = (0, \pi)$ and $Y = (0, \pi) \rightarrow \Gamma = (0, 0)$) for $U = 8$, $n = 0.78$ and $T = 0.01$ (top panel), $n = 0.85$ and $T = 0.01$ (middle panel) and $n = 0.92$ and $T = 0.02$ (bottom panel) in proximity of the chemical potential. The dashed lines are labeled with the values of $\Sigma''(\mathbf{k}, \omega)$. The dashed-dotted line is a guide to the eye and marks the direction of the dispersion just *before* the kink. The presence of kinks in the dispersion in both the nodal ($\Gamma = (0, 0) \rightarrow M = (\pi, \pi)$) and the antinodal ($X = (\pi, 0) \rightarrow \Gamma = (0, 0)$) directions is quite evident and signals the coupling of the electrons to a bosonic mode as reported by ARPES experiments [1]. In our formulation, the mode is clearly magnetic. The extension of the flat region in the dispersion around the antinodal points increases systematically on decreasing doping. This clearly signals the transfer of spectral weight from the Fermi surface as it is destroyed by strong correlations (see Fig. 4).

In conclusion, we have shown how a pseudogap scenario and non-Fermi-liquid features can be obtained in

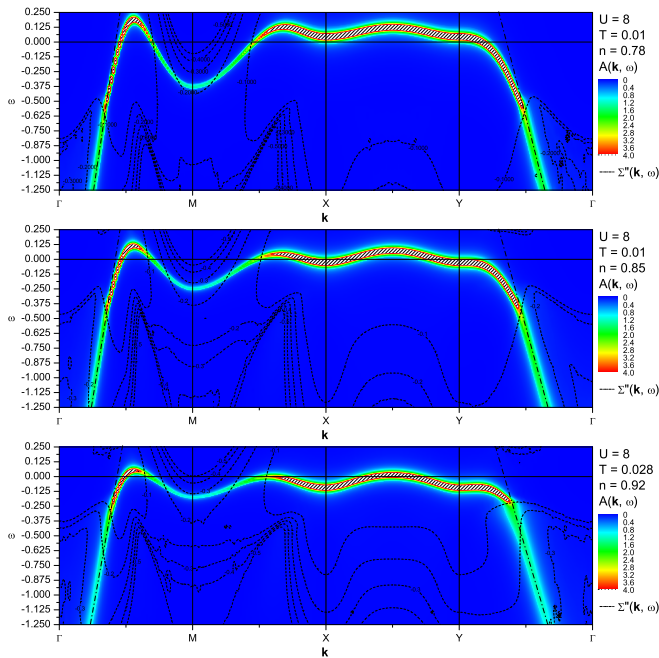


FIG. 5: Spectral function $A(\mathbf{k}, \omega)$ along principal directions for $U = 8$, (left) $n = 0.78$ and $T = 0.01$ (center) $n = 0.85$ and $T = 0.01$ (right) $n = 0.92$ and $T = 0.028$.

the 2D Hubbard model within the Composite Operator Method with the electronic self-energy computed in the Self-Consistent Born Approximation. This scenario is just the one recently claimed for underdoped Cuprates by ARPES experiments [1]. In particular, we report: formation of a pseudogap with related *hot* and *cold* spots and *arcs* on the Fermi surface; non-Fermi liquid features such as the non coincidence of the level 0.5 of the momentum distribution function and the effective Fermi surface and as the absence of a jump in the momentum distribution function at the level 0.5; kinks in the dispersion along nodal and anti-nodal directions. We are now planning to compute the residual self-energy of the bosonic

propagators and to take into account the next-nearest-neighbor hopping term in the Hamiltonian in order to make quantitative comparisons with experiments.

We wish to gratefully acknowledge many useful discussions with N. M. Plakida and P. Prelovsek.

* E-mail: avella@sa.infn.it

† E-mail: mancini@sa.infn.it; Group Homepage: <http://scs.sa.infn.it>

- [1] A. Damascelli, Z. Hussain, and Z.-X. Shen, Rev. Mod. Phys. **75**, 473 (2003).
- [2] T. Timusk and B. Statt, Rep. Prog. Phys. **62**, 61 (1999).
- [3] M. Eschrig, Adv. Phys. **55**, 47 (2006).
- [4] P. A. Lee, N. Nagaosa, and X.-G. Wen, Rev. Mod. Phys. **78**, 17 (2006).
- [5] A.-M. S. Tremblay, B. Kyung, and D. Sénéchal, **32**, 561 (2006).
- [6] P. W. Anderson, Science **235**, 1196 (1987).
- [7] J. Hubbard, Proc. Roy. Soc. A **276**, 238 (1963).
- [8] N. Bulut, Adv. Phys. **51**, 1587 (2002).
- [9] G. Kotliar, S. Y. Savrasov, G. Pallson, and G. Biroli, Phys. Rev. Lett. **87**, 186401 (2001).
- [10] M. H. Hettler, A. N. Tahvildar-Zadeh, M. Jarrell, T. Pruschke, and H. R. Krishnamurthy, Phys. Rev. B **58**, R7475 (1998).
- [11] D. Sénéchal, D. Perez, and M. Pioro-Ladrière, Phys. Rev. Lett. **84**, 522 (2000).
- [12] F. Mancini and A. Avella, Adv. Phys. **53**, 537 (2004).
- [13] J. Bosse, W. Götze, and M. Lücke, Phys. Rev. A **17**, 434 (1978).
- [14] A. Avella, S. Krivenko, F. Mancini, and N. M. Plakida, J. Magn. Magn. Mat. **272**, 456 (2004).
- [15] S. Krivenko, A. Avella, F. Mancini, and N. Plakida, Physica B **359-361**, 666 (2005).
- [16] A. Avella, F. Mancini, and V. Turkowski, Phys. Rev. B **67**, 115123 (2003).
- [17] N. M. Plakida and V. S. Oudovenko (2006), preprint JINR, E-17-2006-96.